ACS Catalysis

Research Article

pubs.acs.org/acscatalysis

Alloyed Co−Mo Nitride as High-Performance Electrocatalyst for Oxygen Reduction in Acidic Medium

Tao Sun,[†] Qiang Wu,*[,†] Renchao Che,[‡] Yongfeng Bu,[†] Yufei Jiang,[†] Yi Li,[†] Lijun Yang,[†] Xizhang Wang,[†] and Zheng Hu*[,†]

[†]Key Laboratory of Mesoscopic Chemistry of MOE and Jiangsu Provincial Laboratory for Nanotechnology, School of Chemistry and Chemical Engineering, Nanjing University, Nanjing 210093, People's Republic of China

[‡]Department of Materials Science and Advanced Materials Laboratory, Fudan University, Shanghai 200433, People's Republic of China

Supporting Information

ABSTRACT: Exploring cheap and stable electrocatalysts to replace Pt for the oxygen reduction reaction (ORR) is now the key issue for the large-scale application of fuel cells. Herein, we report an alloyed Co−Mo nitride electrocatalyst supported on nitrogen-doped carbon nanocages (NCNCs) which combines the merits of cobalt nitride and molybdenum nitride, showing high activity comparable to that of cobalt nitride and progressively enhanced stability with the increase in the Mo ratio. The typical $Co_{0.5}Mo_{0.5}N_y$/NCNCs catalyst demonstrates excellent ORR performance in acidic medium with a high onset potential of 808 mV vs RHE, superior stability (>80% retention after 100 h of continuous testing in 0.5 mol L^{-1} H_2SO_4), a dominant four-electron catalytic process, and good immunity to methanol crossover. Together with the convenient and scalable preparation as well as the low cost, the alloyed Co−Mo nitride electrocatalyst shows great potential in application for fuel cells. This study also suggests a promising strategy to develop non-precious-metal ORR electrocatalysts in acidic medium: i.e., to construct the alloyed compounds by combining substances with respective high activity and high stability.

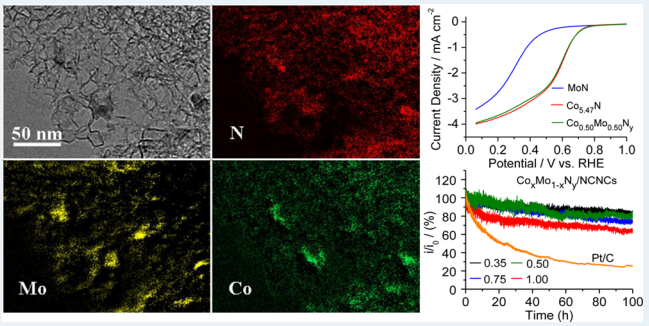

KEYWORDS: *alloyed Co−Mo nitride, oxygen reduction reaction, nonprecious metal, acidic medium, electrocatalysts*

INTRODUCTION

The growing energy and environmental crises have been promoting the efficient utilization of fossil fuels and the exploration of renewable alternative energies. Fuel cells can efficiently convert chemical energy stored in biomass-derived fuels (such as methanol and H_2) into electrical energy in a green manner. In comparison with the oxidation reaction of fuels at the anode, the oxygen reduction reaction (ORR) at the cathode is the main bottleneck, due to its sluggish kinetics.[1] Platinum and its alloys have so far been demonstrated to be the most active ORR catalysts.[1,2] However, their prohibitive cost, scarcity, deactivation by CO poisoning, and fuel crossover effect have hindered the large-scale application of fuel cells. In recent years, great progress has been achieved in exploring non-precious-metal (NPM) ORR electrocatalysts,[3−5] especially in developing cheap transition-metal oxides[4] and metal-free carbon-based nanostructures.[5] However, most of these new ORR electrocatalysts are promising only in alkaline medium. In acidic medium the metal oxide electrocatalysts are prone to dissolution, while the metal-free carbon-based nanostructures show poor ORR activity.[5d,e,h] As is known, fuel cells working in alkaline medium are troubled by carbonate precipitation due to the unavoidable reaction of the electrolyte with the omnipresent CO_2.[6] In contrast, fuel cells working in an acidic medium are naturally CO_2 tolerant with high volumetric power and well-developed acidic membrane electrolyte and are close to practical application.[7] Therefore, developing NPM electrocatalysts for ORR in acidic medium is of practical significance and is highly desired.

To date, three families of alternative ORR electrocatalysts in acidic medium are impressive: (1) Fe(Co)/N/C-based macrocyclic compounds,[8] conductive polymers,[9] or their pyrolyzing derivative,[10] (2) NPM-based chalcogenides,[11] and (3) NPM-based nitrides and oxynitrides.[12] Briefly, the Fe(Co)/N/C-based macrocyclic compounds or conductive polymers show considerable ORR activity but decay easily due to their structural instability.[13] Their pyrolyzed derivatives exhibit superior performance, even rivaling that of commercial Pt/C in onset potential and durability.[10a] Numerous studies have followed this breakthrough, but the resultant catalysts could not reach the expected performance,[10c,14] due to difficulties in the synthesis chemistry.[15] NPM-based chalcogenides such as CoS_2

Received: December 17, 2014
Revised: February 5, 2015
Published: February 12, 2015

DOI: 10.1021/cs502029h
ACS Catal. 2015, 5, 1857−1862

and Co_3S_4 present a modest ORR activity with an onset potential of 0.6−0.8 V vs RHE, but the stability is far from satisfactory.[16] In contrast, NPM-based nitrides/oxynitrides such as molybdenum nitride and tantalum oxynitride show superb stability due to their high resistance to acidic solution and high immunity to methanol, but their activity is not attractive.[12c−f] Recently, we found that cobalt nitride has high ORR activity in acidic medium but is not very stable. By combining the merits of the high activity of cobalt nitride and the superb stability of molybdenum nitride, in this study we have developed an alloyed cobalt−molybdenum nitride electrocatalyst which demonstrates high activity and stability for the ORR in acidic medium. This result suggests a prospective strategy to explore advanced hybrid ORR electrocatalysts in acidic medium by integrating the respective advantages of the individual components.

EXPERIMENTAL SECTION

Synthesis of Alloyed Co−Mo Nitride Electrocatalysts. The N-doped carbon nanocage (NCNC) support was prepared at 800 °C by an in situ MgO template method, and the specific surface area is 843 $m^2\ g^{-1}$.[17] The $Co_xMo_{1-x}N_y$/NCNC hybrid catalysts were synthesized by a convenient impregnation and nitridation method. In a typical run, 50 mg of the NCNCs was dispersed ultrasonically into deionized water, and then an appropriate amount of cobalt nitrate ($Co(NO_3)_2{\cdot}6H_2O$) and/or ammonium molybdate ($(NH_4)_6Mo_7O_{24}{\cdot}4H_2O$) was dissolved with stirring. After the water was evaporated at 70 °C, the dried powders were placed in a tubular furnace for nitridation. Under an NH_3 flow of 50 sccm, the samples were heated to 350 °C at a rate of 5 °C min^{-1} and then to 700 °C at 2.5 °C min^{-1}, kept there for 3 h, and then cooled to room temperature. The loading is defined as the weight ratio of the metal species to the NCNC support, i.e., $weight_{Co+Mo}/weight_{NCNC}$, which was adjusted in the range of 0−50 wt %.

Characterization. The catalysts were characterized by X-ray diffraction (XRD, Philips X'pert Pro X-ray diffractometer with Cu Kα radiation), transmission electron microscopy (TEM, JEM-2100), inductively coupled plasma−mass spectroscopy (ICP-MS, Optima 5300DV), and X-ray photoelectron spectroscopy (XPS, VG ESCALAB MKII). The binding energies of XPS spectra refer to C 1s at 284.6 eV. The specific surface area and pore volume of the NCNCs were measured with a Micromeritics ASAP 2010 instrument at 77 K with N_2 as absorbate.

Electrochemical Measurements. The electrochemical tests including cyclic voltammetry (CV) and rotating disk electrode (RDE) and rotating ring disk electrode (RRDE) voltammetry were performed on an MSR electrode rotator (Pine Instrument Co.) coupled with a CHI 760C workstation (CH Instruments) with the counter electrode of Pt wire and the reference electrode of Ag/AgCl (3 M KCl). Briefly, the catalyst inks were prepared by adding 2 mg of $Co_xMo_{1-x}N_y$/NCNC powder to a mixture of 0.80 mL of water, 0.20 mL of ethanol, and 40 μL of Nafion (Dupont, 5 wt %) with 1 h ultrasonic treatment. A 10 μL portion of fresh catalyst ink was dropped onto a glassy-carbon electrode (GC; 0.196 cm^2, Pine Instrument Co.) and dried at room temperature for 12 h. Thus, the catalyst loading on the GC electrodes was 0.097 mg cm^{-2}. The same loading was used for the commercial Pt/C (20 wt % Pt) catalyst for comparison. The CV, RDE, and RRDE curves were recorded in O_2-saturated 0.5 mol L^{-1} H_2SO_4 at a scan rate of 10 mV s^{-1}, and the Pt ring electrode was polarized at 1.0 V vs Ag/AgCl. The electron transfer number (n) and the corresponding H_2O_2 yield were calculated by $n = 4I_{disk}/(I_{disk} + I_{ring}/N)$ and H_2O_2 (%) $= (200I_{ring}/N)/(I_{disk} + I_{ring}/N)$, where I_{disk} and I_{ring} were the disk electrode current and ring electrode current, respectively, and N was the collection efficiency at the ring electrode (N = 0.26). The chronoamperometric response was tested for 100 h in the O_2-saturated electrolyte by constantly bubbling O_2 (15 mL min^{-1}) with magnetic stirring during the whole process. In the methanol crossover tests, 2% (v/v) methanol was introduced into O_2-saturated electrolyte at 1200 s.

RESULTS AND DISCUSSION

The NCNCs with a specific surface area of 843 $m^2\ g^{-1}$ were used as the support (SI 1 in the Supporting Information).[17] By adjustment of the loading and ratio of cobalt salts and molybdenum salts, two series of $Co_xMo_{1-x}N_y$/NCNC electrocatalysts ($y \leq 1$) were prepared: i.e., with tunable loading of 5−50 wt % at x = 0.50 and tunable x of 0−1.00 at 10 wt % loading, respectively.

ORR activities of these hybrid electrocatalysts were measured by CV and RDE voltammetry in O_2-saturated 0.5 mol L^{-1} H_2SO_4 solution (Figure 1 and SI 2 in the Supporting

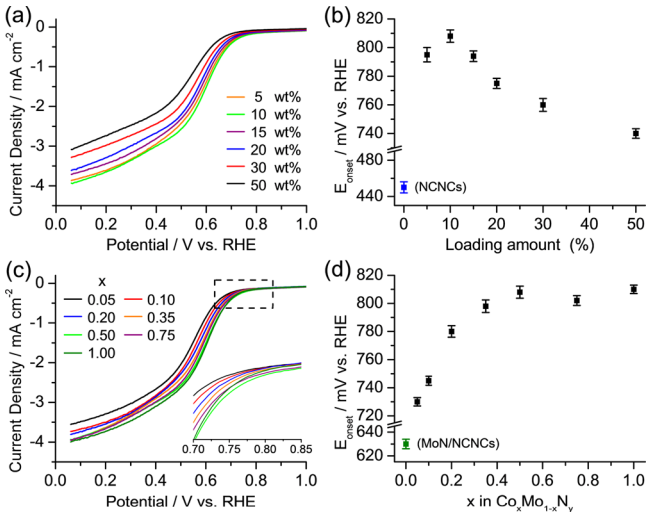

Figure 1. ORR performance of the two series of $Co_xMo_{1-x}N_y$/NCNCs catalyst: (a, b) RDE curves (a) and derived onset potentials vs loading (b) for the $Co_{0.50}Mo_{0.50}N_y$/NCNCs; (c, d) RDE curves (c) and the derived onset potentials vs the x value (d) for the $Co_xMo_{1-x}N_y$/NCNCs with 10 wt % loading. The inset in (c) is the local enlargement. For comparison, the onset potentials for the NCNCs and MoN/NCNCs are depicted in (b) and (d), respectively. The error bars in (b) and (d) are the standard deviations on the basis of three groups of samples.

Information). Figure 1 displays the ORR performances of the two series of $Co_xMo_{1-x}N_y$/NCNC catalysts. The onset potentials (E_{onset}), i.e. the separating point of RDE (or CV) curves measured in O_2- and N_2-saturated solutions, and current densities (i) at 0.5 V (vs RHE) change with increasing loading of the $Co_{0.50}Mo_{0.50}N_y$/NCNC (Figure 1a,b). The optimized loading is 10 wt %, at which E_{onset} reaches the maximum of 808 mV (much higher than 450 mV for the NCNCs) and i of 2.56 mA cm^{-2} (Figure S2 in the Supporting Information). With this optimal loading, the effect of Co content on ORR performance for $Co_xMo_{1-x}N_y$ has been examined. The participation of Co

DOI: 10.1021/cs502029h
ACS Catal. 2015, 5, 1857−1862

leads to a hasty increase of E_{onset} from 630 mV for MoN/NCNC to ~800 mV for $Co_{0.35}Mo_{0.65}N_y$ and then stays at this high level over the wide x range of 0.35−1.00 (Figure 1c,d). The optimization study indicates that the $Co_xMo_{1-x}N_y$/NCNC hybrids with $x \geq 0.35$ have a high onset potential of ~800 mV for the ORR in 0.5 mol L^{-1} H_2SO_4, which is superior to those of the state-of-the-art NPM-based nitride, oxynitride, and chalcogenide catalysts in acidic medium (Table S1 in the Supporting Information). In addition, the ORR performance is insensitive to the composition over a wide range, which implies the high reproducibility by a convenient preparation. In this aspect it is superior to the Fe/N/C or Co/N/C moieties, whose performance highly depends on the preparation procedures.[15]

As a representative, the bimetallic $Co_{0.50}Mo_{0.50}N_y$/NCNCs with 10 wt % loading has been characterized in detail, with the monometallic MoN/NCNCs and $Co_{5.47}N$/NCNCs for comparison. Figure 2 shows TEM characterization results of the

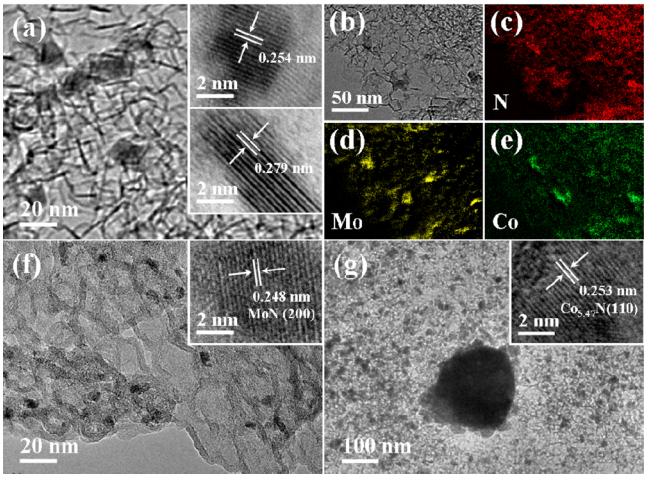

Figure 2. TEM characterization of the $Co_{0.50}Mo_{0.50}N_y$/NCNC, MoN/NCNC, and $Co_{5.47}N$/NCNC catalysts: (a) $Co_{0.50}Mo_{0.50}N_y$/NCNC; (b−e) low-magnification TEM image (b) and corresponding elemental mapping (c−e) of the $Co_{0.5}Mo_{0.5}N_y$/NCNCs; (f) MoN/NCNC; (g) $Co_{5.47}N$/NCNC. All insets are HRTEM images of the corresponding samples.

samples. The MoN particles are highly dispersed on the NCNC support with sizes of 2−7 nm. High-resolution TEM (HRTEM) showed the lattice fringes with a spacing of 0.248 nm corresponding to the (200) plane of MoN (Figure 2f and Figure S3a−d in the Supporting Information). In contrast, the $Co_{5.47}N$ particles present a bimodal distribution with sizes of 5−25 and 50−250 nm (SI 3 in the Supporting Information). HRTEM observed the lattice fringes with a spacing of 0.253 nm in consistence with the (110) plane of $Co_{5.47}N$ (Figure 2g and Figure S3e−h in the Supporting Information). The bimetallic $Co_{0.50}Mo_{0.50}N_y$ particles mainly distribute in the range of 8−18 nm without abnormally large particles, generally between the sizes of MoN and $Co_{5.47}N$, suggesting the uniform dispersion of the Co species due to the Mo participation (Figure 2a). HRTEM showed two kinds of crystal lattices with spacings of 0.279 and 0.254 nm, which cannot be assigned to MoN or $Co_{5.47}N$ and indicate the formation of the bimetallic Co−Mo nitride (inset in Figure 2a and Figure S3i−l in the Supporting Information). The elemental mapping presents the similar dispersion of Co, Mo, and N species (Figure 2b−e), supporting the HRTEM result. XRD and energy dispersive spectroscopy (EDS) characterizations also give similar results (SI 4 in the Supporting Information).

The evolution of XPS spectra for the $Co_xMo_{1-x}N_y$/NCNCs is shown in Figure 3 with x increasing from 0 to 1.00. For the MoN/NCNCs (x = 0), the main peaks of Mo $3d_{5/2}$ appear at 231.80 and 232.47 eV, coming from the dominant Mo^{6+} and minor Mo^{5+} species.[18] In the corresponding N 1s spectrum, there exists a decomposed peak (N3) at 397.90 eV resulting from the supported MoN nanoparticles,[18c] in addition to the peaks of pyridinic N (N2, at 398.53 eV) and graphitic N (N1, at 400.82 eV) from the NCNC support.[17] The incorporation of Co leads to the appearance of a new Mo^{3+} species at 229.20 ± 0.10 eV.[18b] With an increase in the Co content (x), the relative content of the Mo^{3+} species increases, accompanied by an increasing Mo^{5+}/Mo^{6+} ratio. Such an evolution indicates electron transfer from the Co species to the Mo species, which results in a decrease in the valence state of Mo species. This result further suggests the alloying of Co and Mo in the $Co_xMo_{1-x}N_y$ catalysts, in agreement with the HRTEM observation and elemental mapping results (Figure 2b−e). Meanwhile, the content of N3 (from the $Co_xMo_{1-x}N_y$) relative to that of N1 and N2 (from the NCNCs) decreases gradually with the binding energy slightly shifting from 397.90 eV for MoN/NCNCs (x = 0), via 397.88 eV (x = 0.10), 397.80 eV (x = 0.50), and 397.74 eV (x = 0.75), to 397.63 eV for $Co_{5.47}N$/NCNCs (x = 1.00).[18b] Taking into account the different nitrogen contents in MoN and $Co_{5.47}N$, the gradual decrease of N3 content in $Co_xMo_{1-x}N_y$/NCNCs with increasing x is a natural result. The Co $2p_{3/2}$ peak appears at 780.73 ± 0.07 eV with a satellite at 786.10 ± 0.07 eV, suggesting the Co^{2+}-like species.[19] XPS analysis reveals a molar ratio of 1.37:1 for Co:Mo in the $Co_{0.50}Mo_{0.50}N_y$/NCNCs. In comparison with the corresponding molar ratio of 0.99:1 detected by ICP-MS (Table S3 in the Supporting Information), this indicates the surface enrichment of Co species in the alloyed Co−Mo nitride particles.

The CV, RDE, and RRDE curves of the catalysts are shown in Figure 4. In comparison with the featureless case in the N_2-saturated solution, an apparent ORR peak appears on the CV curve at 316 mV (vs RHE) for MoN/NCNC, 621 mV for $Co_{0.50}Mo_{0.50}N_y$/NCNC, and 626 mV for $Co_{5.47}N$/NCNC in O_2-saturated solutions (Figure 4a). The corresponding onset potentials (E_{onset}) are ~630, ~808, and ~810 mV, respectively, as confirmed by the RDE measurements (Figure 4a,b). The alloyed $Co_{0.50}Mo_{0.50}N_y$/NCNC displays an ORR performance comparable with that of the $Co_{5.47}N$/NCNCs and much better than that of the MoN/NCNCs and the NCNCs. E_{onset} for the $Co_{0.50}Mo_{0.50}N_y$/NCNCs (~808 mV) is only ~147 mV lower than 955 mV for the commercial Pt/C catalyst (Figure S2e,f in the Supporting Information). The electron transfer number (n) and the corresponding H_2O_2 yield during the ORR are calculated to be ~3.75 ± 0.10 and ~12.6% in the range of 0.05−0.60 V, indicating a dominant four-electron process (Figure 4c,d). The n value is slightly lower than that of the $Co_{5.47}N$/NCNCs but obviously higher than that of the MoN/NCNCs (Figure 4d and Table S2 in the Supporting Information). These results indicate that the high ORR activity can be mainly attributed to the cobalt-containing nitride nanoparticles.[20]

The long-term ORR stability of the optimized bimetallic $Co_xMo_{1-x}N_y$/NCNC (x = 0.35−1.00) catalysts have been evaluated by chronoamperometric responses, as shown in

DOI: 10.1021/cs502029h
ACS Catal. 2015, 5, 1857−1862

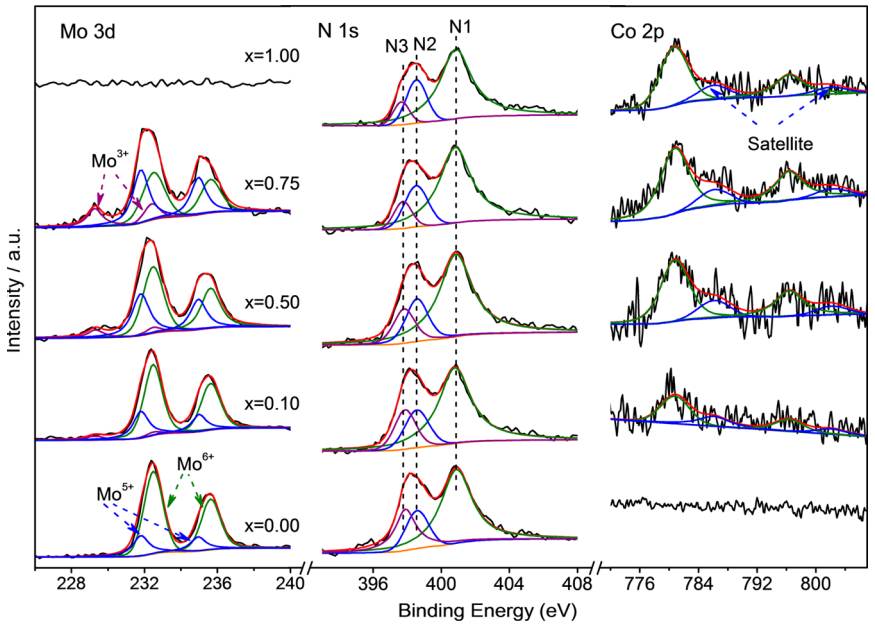

Figure 3. Evolution of XPS spectra for the $Co_xMo_{1-x}N_y$/NCNCs catalysts with increasing x from 0 to 1.00. N1 (400.85 ± 0.05 eV), N2 (398.50 ± 0.05 eV), and N3 (397.63−397.90 eV) correspond to graphitic N, pyridinic N, and nitrides, respectively.

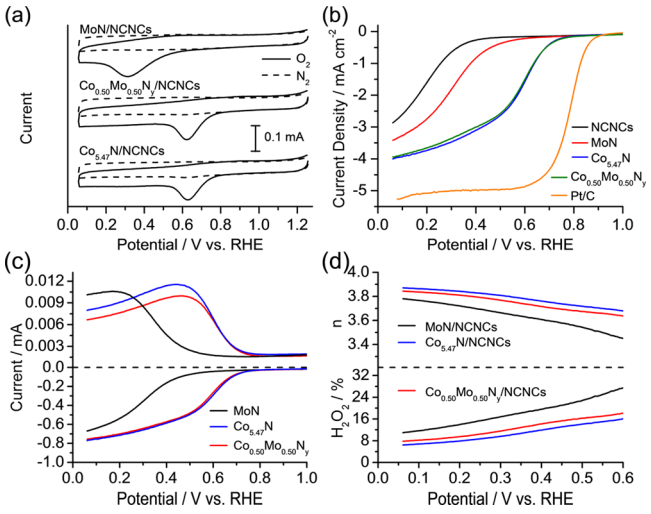

Figure 4. ORR performances of the $Co_{0.50}Mo_{0.50}N_y$/NCNC, MoN/NCNC, and $Co_{5.47}N$/NCNC catalysts in 0.5 mol L^{-1} H_2SO_4: (a) CV curves in N_2-saturated (- - -) and O_2-saturated (—) H_2SO_4 solutions; (b) RDE curves; (c) RRDE curves; (d) electron transfer number (n) and H_2O_2 yield vs potential. For comparison, the RDE curves for NCNCs and commercial Pt/C (20 wt % Pt) are depicted. CV was carried out at a scan rate of 10 mV s^{-1}. The rotating speed for the RDE or RRDE was 2500 rpm. The RDE test of Pt/C was performed in 0.1 mol L^{-1} $HClO_4$ with a rotating speed of 1600 rpm.

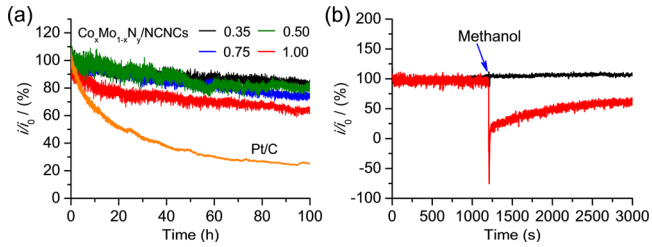

Figure 5. Chronoamperometric responses of the $Co_xMo_{1-x}N_y$/NCNCs catalysts: (a) stability test for 100 h; (b) methanol crossover test by addition of 2% (v/v) methanol to the electrochemical cell at 1200 s as shown by an arrow. The tests were performed in O_2-saturated 0.5 mol L^{-1} H_2SO_4 with magnetic stirring. The corresponding tests for the commercial Pt/C (20 wt % Pt) catalyst were performed in O_2-saturated 0.1 mol L^{-1} $HClO_4$. In (a), the bias voltage was set at 0.2 V (vs Ag/AgCl). In (b), the bias voltage was set at 0.3 V for $Co_xMo_{1-x}N_y$/NCNC and 0.4 V for Pt/C, respectively. i_0 defines the initial current.

Figure 5. The retention of the ORR current increases with the increase in the Mo species. The $Co_{0.35}Mo_{0.65}N_y$/NCNC catalyst (x = 0.35) exhibits the best stability with a decrease of ~16% after 100 h of testing, much smaller than the ~36% decrease for $Co_{5.47}N$/NCNC and ~75% for Pt/C (Figure 5a and SI 5 in the Supporting Information). The superior ORR stability for the bimetallic nitride $Co_xMo_{1-x}N_y$/NCNC mainly results from its much improved resistance to acidic medium due to the alloying of Co and Mo, while the inferior stability of $Co_{5.47}N$/NCNC is due to the dissolution of the $Co_{5.47}N$ particles in acid solution (Table S4 and Figure S11 in the Supporting Information). In comparison with the small particles, the large particles in the $Co_{5.47}N$/NCNCs are more easily dissolved in acid (Figure S10 in the Supporting Information). The bimetallic $Co_xMo_{1-x}N_y$/NCNC catalyst also exhibits superb tolerance to methanol crossover. By addition of 2% (v/v) methanol to the solution during the chronoamperometric tests, the current for $Co_{0.50}Mo_{0.50}N_y$/NCNC stays constant while that for Pt/C suffers a sharp decrease (Figure 5b).

As indicated by the comparison, the alloyed Co−Mo nitrides can mostly preserve the ORR activity of cobalt nitride in both E_{onset} and current density, while presenting relatively good ORR stability due to the Mo participation (Figures 4b and 5). The alloyed Co−Mo nitride sample has smaller particle sizes and narrower distribution in comparison to the cobalt nitride, free from serious aggregation as the case for the $Co_{5.47}N$ sample (Figure 2a,g), as well as the surface enrichment of Co species, which promotes the efficiency of the cobalt usage. In addition, the Mo species enhances the resistance of the alloyed Co−Mo nitride to acidic medium (Figure 5a and Table S3 in the

DOI: 10.1021/cs502029h
ACS Catal. 2015, 5, 1857−1862

Supporting Information). Hence, the alloyed $Co_xMo_{1-x}N_y$/NCNC catalysts ($x \geq 0.35$) integrate the merits of highly active $Co_{5.47}N$/NCNCs and highly stable MoN/NCNCs and avoid the drawbacks of poorly active MoN/NCNCs and poorly stable $Co_{5.47}N$/NCNCs. This might be an effective strategy to develop NPM-based advanced electrocatalysts in acidic medium, which has been successfully extended to other material systems: e.g., the bimetallic $CoMoS_{3.13}$/NCNCs catalyst also combines the high ORR activity of CoS_x and good ORR stability of MoS_2 (SI 6 in the Supporting Information).

CONCLUSION

In summary, the alloyed $Co_xMo_{1-x}N_y$/NCNCs have been applied as cheap ORR electrocatalysts in acidic medium; they exhibit excellent ORR performance, including the dominant 4e catalytic process, high activity, superior stability, and immunity to methanol crossover. The alloyed Co−Mo nitrides, evidenced by the emergence of the new Mo^{3+} species, combine the merits of the high activity of cobalt nitride and the high stability of molybdenum nitride, while avoiding their respective drawbacks of low stability and low activity. The narrowly distributed sizes of the bimetallic nitride are between those of the small MoN and the large $Co_{5.47}N$: i.e., the Mo participation can effectively increase the usage efficiency of the active Co species. Together with the convenient and scalable synthesis as well as the low cost, the alloyed Co−Mo nitride electrocatalysts exhibit great potential in applications for proton exchange membrane fuel cells. This study also suggests a promising strategy to explore non-precious-metal ORR electrocatalysts in acidic medium, i.e., to construct the alloyed compounds by combining substances with respective high activity and high stability.

ASSOCIATED CONTENT

Supporting Information

The following file is available free of charge on the ACS Publications website at DOI: 10.1021/cs502029h.

Characterization of the NCNCs and the series of $Co_xMo_{1-x}N_y$/NCNC electrocatalysts, additional characterizations of other control catalysts, additional electrochemical results, and a performance comparison with the literature (PDF)

AUTHOR INFORMATION

Corresponding Authors

*E-mail for Q.W.: wqchem@nju.edu.cn.
*E-mail for Z.H.: zhenghu@nju.edu.cn.

Notes

The authors declare no competing financial interest.

ACKNOWLEDGMENTS

This work was jointly supported by the NSFC (51232003, 21073085, 21173115, 21473089), the "973" program (2013CB932902), Jiangsu Province Science and Technology Support Project (BE2012159), and Suzhou Science and Technology Plan Projects (ZXG2013025).

REFERENCES

(1) (a) Gasteiger, H. A.; Markovic, N. M. *Science* **2009**, *324*, 48−49. (b) Gewirth, A. A.; Thorum, M. S. *Inorg. Chem.* **2010**, *49*, 3557−3566.
(2) (a) Wu, J. B.; Yang, H. *Acc. Chem. Res.* **2013**, *46*, 1848−1857. (b) Chen, C.; Kang, Y. J.; Huo, Z. Y.; Zhu, Z. W.; Huang, W. Y.; Xin, H. L.; Snyder, J. D.; Li, D. G.; Herron, J. A.; Mavrikakis, M.; Chi, M. F.; More, K. L.; Li, Y. D.; Markovic, N. M.; Somorjai, G. A.; Yang, P. D.; Stamenkovic, V. R. *Science* **2014**, *343*, 1339−1343. (c) Lim, B. K.; Jiang, M. J.; Camargo, P. H. C.; Cho, E. C.; Tao, J.; Lu, X. M.; Zhu, Y. M.; Xia, Y. N. *Science* **2009**, *324*, 1302−1305. (d) Wang, D. L.; Xin, H. L.; Hovden, R.; Wang, H. S.; Yu, Y. C.; Muller, D. A.; DiSalvo, F. J.; Abruña, H. D. *Nat. Mater.* **2013**, *12*, 81−87. (e) Guo, S. J.; Li, D. G.; Zhu, H. Y.; Zhang, S.; Markovic, N. M.; Stamenkovic, V. R.; Sun, S. H. *Angew. Chem., Int. Ed.* **2013**, *52*, 3465−3468. (f) Zhang, L.; Iyyamperumal, R.; Yancey, F. Y.; Crooks, R. M.; Henkelman, G. *ACS Nano* **2013**, *7*, 9168−9172. (g) Negro, E.; Vezzù, K.; Bertasi, F.; Schiavuta, P.; Toniolo, L.; Polizzi, S.; Noto, V. D. *ChemElectroChem* **2014**, *1*, 1359−1369. (h) Negro, E.; Schiavuta, P.; Vezzù, K.; Toniolo, L.; Cavinato, G.; Noto, V. D. *Int. J. Hydrogen Energy* **2014**, *39*, 2828−2841. (i) Negro, E.; Noto, V. D. *J. Power Sources* **2008**, *178*, 634−641. (j) Jiang, S. J.; Ma, Y. W.; Jian, G. Q.; Tao, H. S.; Wang, X. Z.; Fan, Y. N.; Lu, Y. N.; Hu, Z.; Chen, Y. *Adv. Mater.* **2009**, *21*, 4953−4956.
(3) (a) Morozan, A.; Jousselme, B.; Palacin, S. *Energy Environ. Sci.* **2011**, *4*, 1238−1254. (b) Yang, Z.; Nie, H. G.; Chen, X. A.; Chen, X. H.; Huang, S. M. *J. Power Sources* **2013**, *236*, 238−249.
(4) (a) Liang, Y. Y.; Li, Y. G.; Wang, H. L.; Dai, H. J. *J. Am. Chem. Soc.* **2013**, *135*, 2013−2036. (b) Liang, Y. Y.; Li, Y. G.; Wang, H. L.; Zhou, J. G.; Wang, J.; Regier, T.; Dai, H. J. *Nat. Mater.* **2011**, *10*, 780−786. (c) Cheng, F. Y.; Shen, J.; Peng, B.; Pan, Y. D.; Tao, Z. L.; Chen, J. *Nat. Chem.* **2011**, *3*, 79−84. (d) Wu, Z. S.; Yang, S. B.; Sun, Y.; Parvez, K.; Feng, X. L.; Müllen, K. *J. Am. Chem. Soc.* **2012**, *134*, 9082−9085. (e) Zhu, H. Y.; Zhang, S.; Huang, Y. X.; Wu, L. H.; Sun, S. H. *Nano Lett.* **2013**, *13*, 2947−2951. (f) Duan, J. J.; Chen, S.; Dai, S.; Qiao, S. Z. *Adv. Funct. Mater.* **2014**, *24*, 2072−2078. (g) Tan, Y. M.; Xu, C. F.; Chen, G. X.; Fang, X. L.; Zheng, N. F.; Xie, Q. J. *Adv. Funct. Mater.* **2012**, *22*, 4584−4591.
(5) (a) Wang, D. W.; Su, D. S. *Energy Environ. Sci.* **2014**, *7*, 576−591. (b) Gong, K. P.; Du, F.; Xia, Z. H.; Durstock, M.; Dai, L. M. *Science* **2009**, *323*, 760−764. (c) Yang, D. S.; Bhattacharjya, D.; Inamdar, S.; Park, J.; Yu, J. S. *J. Am. Chem. Soc.* **2012**, *134*, 16127−16130. (d) Yu, D. S.; Zhang, Q.; Dai, L. M. *J. Am. Chem. Soc.* **2010**, *132*, 15127−15129. (e) Wei, W.; Liang, H. W.; Parvez, K.; Zhang, X. D.; Feng, X. L.; Müllen, K. *Angew. Chem., Int. Ed.* **2014**, *53*, 1570−1574. (f) Liang, J.; Jiao, Y.; Jaroniec, M.; Qiao, S. Z. *Angew. Chem., Int. Ed.* **2012**, *51*, 11496−11500. (g) Chen, P.; Xiao, T. Y.; Qian, Y. H.; Li, S. S.; Yu, S. H. *Adv. Mater.* **2013**, *25*, 3192−3196. (h) Ozaki, J. I.; Kimura, N.; Anahara, T.; Oya, A. *Carbon* **2007**, *45*, 1847−1853. (i) Zhao, Y.; Yang, L. J.; Chen, S.; Wang, X. Z.; Ma, Y. M.; Wu, Q.; Jiang, Y. F.; Qian, W. J.; Hu, Z. *J. Am. Chem. Soc.* **2013**, *135*, 1201−1204. (j) Yang, L. J.; Jiang, S. J.; Zhao, Y.; Zhu, L.; Chen, S.; Wang, X. Z.; Wu, Q.; Ma, J.; Ma, Y. W.; Hu, Z. *Angew. Chem., Int. Ed.* **2011**, *50*, 7132−7135.
(6) (a) Naughton, M. S.; Brushett, F. R.; Kenis, P. J. A. *J. Power Sources* **2011**, *196*, 1762−1768. (b) Tewari, A.; Sambhy, V.; Macdonald, M. U.; Sen, A. *J. Power Sources* **2006**, *153*, 1−10.
(7) (a) Sandstede, G.; Cairns, E. J.; Bagotsky, V. S.; Wiesener, K. In *Handbook of Fuel Cells*; Wiley: Hoboken, NJ, 2010. (b) Noto, V. D.; Piga, M.; Giffin, G. A.; Negro, E.; Furlan, C.; Vezzù, K. *ChemSusChem* **2012**, *5*, 1758−1766.
(8) (a) Li, W. M.; Yu, A. P.; Higgins, D. C.; Llanos, B. G.; Chen, Z. W. *J. Am. Chem. Soc.* **2010**, *132*, 17056−17058. (b) Jahan, M.; Liu, Z. L.; Loh, K. P. *Adv. Funct. Mater.* **2013**, *23*, 5363−5372. (c) Zhang, W.; Shaikh, A. U.; Tsui, E. Y.; Swager, T. M. *Chem. Mater.* **2009**, *21*, 3234−3241.
(9) Bashyam, R.; Zelenay, P. *Nature* **2006**, *443*, 63−66.
(10) (a) Wu, G.; More, K. L.; Johnston, C. M.; Zelenay, P. *Science* **2011**, *332*, 443−447. (b) Lefèvre, M.; Proietti, E.; Jaouen, F.; Dodelet, J. P. *Science* **2009**, *324*, 71−74. (c) Zhao, D.; Shui, J. L.; Grabstanowicz, L. R.; Chen, C.; Commet, S. M.; Xu, T.; Lu, J.; Liu, D. J. *Adv. Mater.* **2014**, *26*, 1093−1097.
(11) (a) Wang, H. L.; Liang, Y. Y.; Li, Y. G.; Dai, H. J. *Angew. Chem., Int. Ed.* **2011**, *50*, 10969−10972. (b) Feng, Y. J.; He, T.; Vante, N. A. *Chem. Mater.* **2008**, *20*, 26−28. (c) Zhu, L.; Susac, D.; Teo, M.; Wong, K. C.; Wong, P. C.; Parsons, R. R.; Bizzotto, D.; Mitchell, K. A. R.; Campbell, S. A. *J. Catal.* **2008**, *258*, 235−242. (d) Feng, Y. J.; He, T.;

DOI: 10.1021/cs502029h
ACS Catal. 2015, 5, 1857−1862

Vante, N. A. *Electrochim. Acta* **2009**, *54*, 5252−5256. (e) Jirkovsky, J. S.; Björling, A.; Ahlberg, E. *J. Phys. Chem. C* **2012**, *116*, 24436−24444. (f) Mahmood, N.; Zhang, C. Z.; Jiang, J.; Liu, F.; Hou, Y. L. *Chem. Eur. J.* **2013**, *19*, 5183−5190.
(12) (a) Cao, B. F.; Veith, G. M.; Diaz, R. E.; Liu, J.; Stach, E. A.; Adzic, R. R.; Khalifah, P. G. *Angew. Chem., Int. Ed.* **2013**, *52*, 10753−10757. (b) Ando, T.; Izhar, S.; Tominaga, H.; Nagai, M. *Electrochim. Acta* **2010**, *55*, 2614−2621. (c) Ishihara, A.; Doi, S.; Mitsushima, S.; Ota, K. I. *Electrochim. Acta* **2008**, *53*, 5442−5450. (d) Qi, J.; Jiang, L. H.; Jiang, Q.; Wang, S. L.; Sun, G. Q. *J. Phys. Chem. C* **2010**, *114*, 18159−18166. (e) Zhong, H. X.; Zhang, H. M.; Liu, G.; Liang, Y. M.; Hu, J. W.; Yi, B. L. *Electrochem. Commun.* **2006**, *8*, 707−712. (f) Xia, D. G.; Liu, S. Z.; Wang, Z. Y.; Chen, G.; Zhang, L. J.; Zhang, L.; Hui, S. Q.; Zhang, J. J. *J. Power Sources* **2008**, *177*, 296−302.
(13) Chen, Z. W.; Higgins, D.; Yu, A. P.; Zhang, L.; Zhang, J. J. *Energy Environ. Sci.* **2011**, *4*, 3167−3192.
(14) (a) Wang, Q.; Zhou, Z. Y.; Lai, Y. J.; You, Y.; Liu, J. G.; Wu, X. L.; Terefe, E.; Chen, C.; Song, L.; Rauf, M.; Tian, N.; Sun, S. G. *J. Am. Chem. Soc.* **2014**, *136*, 10882−10885. (b) Lin, L.; Zhu, Q.; Xu, A. W. *J. Am. Chem. Soc.* **2014**, *136*, 11027−11033. (c) Liang, H. W.; Wei, W.; Wu, Z. S.; Feng, X. L.; Müllen, K. *J. Am. Chem. Soc.* **2013**, *135*, 16002−16005. (d) Yuan, S. W.; Shui, J. L.; Grabstanowicz, L.; Chen, C.; Commet, S.; Reprogle, B.; Xu, T.; Yu, L. P.; Liu, D. J. *Angew. Chem., Int. Ed.* **2013**, *52*, 8349−8353. (e) Wu, Z. S.; Chen, L.; Liu, J. Z.; Parvez, K.; Liang, H. W.; Shu, J.; Sachdev, H.; Graf, R.; Feng, X. L.; Müllen, K. *Adv. Mater.* **2014**, *26*, 1450−1455. (f) Parvez, K.; Yang, S. B.; Hernandez, Y.; Winter, A.; Turchanin, A.; Feng, X. L.; Müllen, K. *ACS Nano* **2012**, *6*, 9541−9550. (g) Byon, H. R.; Suntivich, J.; Horn, Y. S. *Chem. Mater.* **2011**, *23*, 3421−3428.
(15) Wu, G.; Zelenay, P. *Acc. Chem. Res.* **2013**, *46*, 1878−1889.
(16) Gao, M. R.; Jiang, J.; Yu, S. H. *Small* **2012**, *8*, 13−27.
(17) Chen, S.; Bi, J. Y.; Zhao, Y.; Yang, L. J.; Zhang, C.; Ma, Y. W.; Wu, Q.; Wang, X. Z.; Hu, Z. *Adv. Mater.* **2012**, *24*, 5593−5597.
(18) (a) Yao, Z. W.; Zhang, X. H.; Peng, F.; Yu, H.; Wang, H. J.; Yang, J. *J. Mater. Chem.* **2011**, *21*, 6898−6902. (b) Hada, K.; Nagai, M.; Omi, S. *J. Phys. Chem. B* **2001**, *105*, 4084−4093. (c) Becue, T.; Manoli, J. M.; Potvin, C.; Mariadassou, G. D. *J. Phys. Chem. B* **1997**, *101*, 6429−6435.
(19) (a) Li, S.; Zhang, L.; Kim, J.; Pan, M.; Shi, Z.; Zhang, J. J. *Electrochim. Acta* **2010**, *55*, 7346−7353. (b) Barreca, D.; Massignan, C.; Daolio, S.; Fabrizio, M.; Piccirillo, C.; Armelao, L.; Tondello, E. *Chem. Mater.* **2001**, *13*, 588−593.
(20) Tominaga, H.; Nagai, M. *Electrochim. Acta* **2009**, *54*, 6732−6739.

DOI: 10.1021/cs502029h
ACS Catal. 2015, 5, 1857−1862